Coverage Probability of Uplink Cellular Networks

Harpreet S. Dhillon, Thomas D. Novlan, Jeffrey G. Andrews

***Abstract*—The cellular uplink has typically been studied using simple Wyner-type analytical models where interference is modeled as a constant or a single random variable, or via complex system-level simulations for a given set of parameters, which are often insufficient to evaluate performance in all operational regimes. In this paper, we take a fresh look at this classic problem using tools from point process theory and stochastic geometry, and develop a new tractable model for the cellular uplink which provides easy-to-evaluate expressions for important performance metrics such as coverage probability. The main idea is to model the locations of mobiles as a realization of a Poisson Point Process where each base station (BS) is located uniformly in the Voronoi cell of the mobile it serves, thereby capturing the dependence in two spatial processes. In addition to modeling interference accurately, it provides a natural way to model per-mobile power control, which is an important aspect of the uplink and one of the reasons why uplink analysis is more involved than its downlink counterpart. We also show that the same framework can be used to study regular as well as irregular BS deployments by choosing an appropriate distribution for the distance of a mobile to its serving BS. We verify the accuracy of this framework with an actual urban/suburban cellular network.**

I. Introduction

Cellular networks are undergoing a paradigm shift from voice-oriented to ubiquitous mobile-broadband data networks. While the downlink of these networks still drives the bandwidth and speed requirements, improvements in uplink performance are becoming increasingly important due to the increasing popularity of symmetric traffic applications like social networking, video-calls, and real-time generation and sharing of media content. The analysis of the uplink requires several fundamental changes as compared to the downlink, nearly all of which make it more challenging. The interference in the uplink is generated by mobile devices distributed throughout the network, as opposed to the downlink where it comes from the fixed locations. As discussed in the sequel, the locations of these mobiles are coupled with the locations of their serving BSs depending upon the cell-association strategy, presenting the first main challenge in the modeling and analysis of uplink. A second challenge is the use of open and closed-loop (possibly fractional) power control to overcome pathloss and large-scale fading (shadowing), which further couples the locations of the mobiles with their serving BSs and makes the transmit power highly variable, leading to a significant change in the interference statistics compared to the downlink [1]. Additionally, both a maximum power constraint and consideration of average transmit power are especially important for battery powered user devices.

H. S. Dhillon, T. D. Novlan and J. G. Andrews are with WNCG, the University of Texas at Austin (email: dhillon@utexas.edu, tdnovlan@utexas.edu, jandrews@ece.utexas.edu). This research has been supported by AT&T Laboratories and by the National Science Foundation CIF-1016649.

A. Related Work

Research on cellular networks has been driven by three main modeling approaches. First is the Wyner model, wherein the gain for the desired link is normalized to unity and the gain from interferers (typically one or two) is assumed to be a constant or modeled as a single random variable [2]. Although it has been popular for information theoretic studies, its accuracy in typical cellular deployment scenarios is questionable due to simplistic notion of interference and hence of Signal-to-interference-plus-noise-ratio (SINR) [3]. A second and in fact ubiquitous approach is to assume that the BSs lie on a grid with their coverage regions modeled as hexagons. Although this deterministic grid model captures spatial dependencies and can be used to gain insights via complex system-level simulations over a limited set of system parameters [4], [5], it lacks tractability and can not be used to provide performance guarantees in all operational regimes. Besides, it is becoming obsolete due to lack of scalability to the current heterogeneous networks, which may additionally include picocells and femtocells [6].

A third and novel approach is to use random spatial models where the BS locations are assumed to form a realization of some random point process, typically Poisson Point Process (PPP) [6], [7]. In addition to being capable of capturing the aforementioned constraints, it is also tractable and hence is an attractive option for analysis. For the downlink, this model was shown to be about as accurate for macrocells as the the grid model [7] and seems to be the only reasonable option for general heterogeneous cellular networks [6]. Very recent work has also attempted to extend this to the uplink by deriving some approximate results for interference limited networks [8]. More accurate random spatial models are also considered in the literature, often at the cost of reduced tractability [9].

B. Contributions

The main contribution is Theorem 1, which gives the uplink coverage probability for a randomly chosen mobile user with fractional power control, which is a general power control framework. Departing slightly from the random spatial models developed in [6], [7], we model the locations of the users (instead of the BSs) as a Poisson Point Process (PPP). In order to capture spatial dependencies, we then assume that the serving BS of each mobile user is located uniformly in its Voronoi cell [10]. The uplink analysis is significantly more involved than its downlink counterpart because the transmit power of a mobile in the uplink depends upon the distance to its serving BS due to the fractional power control and it turns out that the random variables denoting this distance for each mobile user are identically distributed but not independent in general due to coupling in the locations. This dependence

is not easy to model accurately and hence leads to some technical challenges in the derivation of the coverage probability. However, we show that this dependence is weak and can be ignored, which improves the tractability of the system model with minimal impact on the accuracy of the results. We then derive easy-to-evaluate integral expressions for the uplink coverage probability of a randomly chosen mobile user. Using the same model for the user locations, we also derive coverage probability expression for "regular" BS deployments, where we assume that a BS is uniformly distributed in a circle around its corresponding mobile (independent of other BSs) instead of being uniformly distributed in its Voronoi cell. Interestingly, this analytical result closely approximates the coverage probability computed numerically for the hexagonal grid model. Using these theoretical results, we then present some system design guidelines by comparing downlink and uplink coverage, and evaluating coverage probability and transmit power utilization as a function of the power control parameters.

II. System Model

We consider the uplink of a cellular network utilizing an orthogonal multiple access technique composed of a single class of BSs, macro BSs for example, and focus on the received SINR at a randomly chosen BS. Fig. 1 gives a visual representation of the uplink system model and relationship between various parameters. The mobile user locations are assumed to form a realization of a spatial PPP [10] with density λ. We assume that a mobile user is connected to the closest BS and that each BS has an active uplink user scheduled. Under such an assumption, it is reasonable to assume that each BS is uniformly distributed in the Voronoi cell of its corresponding mobile user. We further assume that the BS chosen at random for analysis is located at the origin and that it connects to the closest mobile user, located at distance R. As discussed in detail in the sequel, there is a subtle difference between this random choice of BS and a point randomly chosen in $\mathbb{R}^2$ due to the coupling in the mobile and BS point processes. The set of interfering mobiles is $\mathcal{Z}_k$, and we denote the distance between an interfering mobile and the BS of interest by D_z and the distance of an interfering mobile to its serving BS as R_z. Path loss is inversely proportional to distance with the path loss exponent given by α, and σ^2 is the noise power. We consider small-scale Rayleigh fading between the mobiles and the BS under consideration, and a constant baseline mobile transmit power of μ^{-1}. Thus the received power is given by $gR^{-\alpha}$, where g is i.i.d exponentially distributed with mean μ^{-1}.

Next we consider the proposed model for power control. We assume that all the mobiles utilize distance-proportional fractional power control of the form $R_z^{\alpha\epsilon}$, where $\epsilon \in [0,1]$ is the power control factor. Thus, as a user moves closer to the desired BS, the transmit power required to maintain the same received signal power decreases, which is an important consideration for battery-powered mobile devices. Under this system model, the associated SINR at a BS located at origin is

$$\mathrm{SINR} = \frac{gR^{\alpha(\epsilon-1)}}{\sigma^2 + I_{\mathcal{Z}}}, \tag{1}$$

where for an interfering set of mobiles $\mathcal{Z}$,

$$I_{\mathcal{Z}} = \sum_{z\in\mathcal{Z}} \left(R_z^{\alpha}\right)^{\epsilon} g_z {D_z}^{-\alpha}. \tag{2}$$

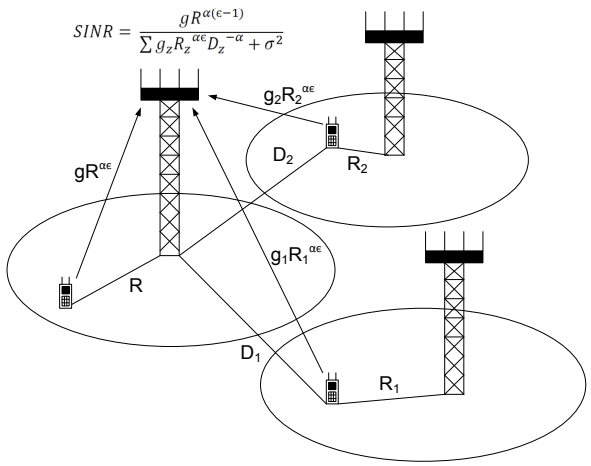

Fig. 1. Visual system model example giving the SINR at BS 0, focusing on the serving mobile and two interfering mobiles in adjacent cells.

If $\epsilon = 1$, the numerator of (1) becomes g, with the pathloss completely inverted by the power control, and if $\epsilon = 0$ no channel inversion is performed and all the mobiles transmit with the same power. In the next section we derive the distribution of the SINR as a function of the network density, pathloss, and fractional power control factor ϵ.

To validate the model and to highlight the importance of various assumptions discussed later in this paper, we will compare the proposed model with various other approaches. For clarity, we describe all these approaches below:

PPP: This corresponds to the proposed model without any assumptions, i.e., mobile locations correspond to a spatial PPP with a single BS dropped uniformly within the Voronoi cell of each mobile. Due to dependence induced by the structure of Poisson-Voronoi tessellation, direct analysis of this approach is daunting and hence not given. Instead several reasonable approximations are made that lead to the following two approaches.

PPP-Rayleigh: Setup is same as the PPP case described above. For tractability we assume i) R is Rayleigh distributed, ii) $\{R_z\}$ are independent, and iii) the marginal distribution of R_z is approximated as Rayleigh.

PPP-Uniform: This model differs from the Rayleigh PPP model in the third assumption, i.e., the marginal distribution of R_z. In this case we assume that the serving BS is located uniformly in a circle centered at the mobile user.

Grid: BSs are located on the centers of a hexagonal grid and one mobile user is distributed uniformly in each cell. Since this model does not lead to tractable expressions it is evaluated via Monte-Carlo simulations.

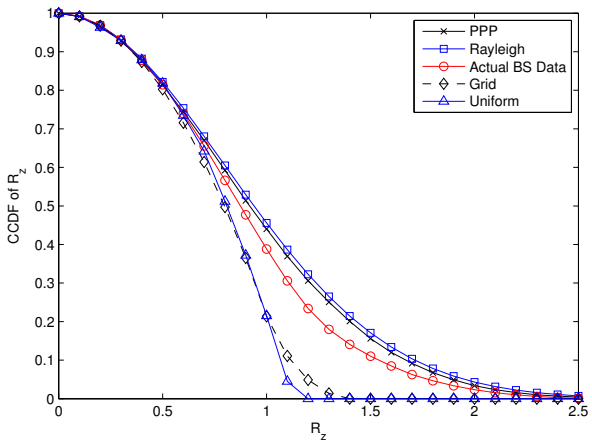

Fig. 2. A comparison of the CCDFs of R_z both for the PPP and a grid model with their respective approximations for $\lambda = 1/4$. Also included is the CCDF of R_z for a set of real BS locations of an urban 4G network.

Wyner: The Wyner model gives a single value for the interference γ which is a function of the pathloss exponent α [3]. The resulting SIR is deterministic and given by $\text{SIR} \equiv \frac{1}{2\gamma}$.

Log-normal: This approach approximates inter-cell interference as a log-normal random variable with parameters determined through a numerical fit using simulations of the grid model.

III. Coverage probability

The probability of coverage can be defined as the complementary cumulative distribution function (ccdf) of SINR as: $p_c = \mathbb{P}[\text{SINR} > T]$. It can also be visualized as being the average area or the average fraction of users in coverage. As noted earlier, we perform analysis on a randomly chosen BS assumed to be located at the origin that connects to the closest mobile user. The distance of the closest mobile from the randomly chosen BS R can be approximated as Rayleigh distributed by the null-probability of a PPP: $\mathbb{P}[R > r] \approx e^{-\lambda \pi r^2}$, which is basically the probability that there is no mobile in the circle of area πr^2. The probability density function (pdf) can now be approximated as

$$f_R(r) \approx 2\pi\lambda r e^{-\lambda \pi r^2}, \; r \geq 0. \tag{3}$$

It should be noted that this is not the exact distribution of R because the randomly chosen BS is not the same as a randomly chosen point in $\mathbb{R}^2$ for which this distribution is exact. This difference comes due to the coupling of mobile and BS point processes. However, as we discuss in detail for R_z, this approximation is tight and does not affect the accuracy of our results.

The net interference at a randomly chosen BS is the sum of the powers from all the transmitting mobiles lying farther than R. As described in the previous section, this power depends upon the distance of a mobile to its corresponding BS and the power control factor $\epsilon \in [0, 1]$. For a mobile $z \in \mathcal{Z}$, we denote its distance to the corresponding BS as R_z. It should be noted that the random variables $\{R_z\}_{z\in\mathcal{Z}}$ are identically distributed but not independent in general. The dependence is induced by the structure of Poisson-Voronoi tessellation and the restriction that only one BS can lie in each Voronoi cell. To visualize this dependence, recall a simple fact that the presence of a BS in a particular Voronoi cell forbids the presence of any other BS in this particular cell. However, as discussed in detail later in this section, this dependence is weak and we will henceforth assume $\{R_z\}$ to be independent and identically distributed (i.i.d.). Under this independence assumption, we first derive the coverage probability for the general distribution of R_z and then use this general result to study two particular scenarios corresponding to non-uniform and regular coverage regions. The main uplink coverage probability result of this paper is stated in Theorem 1.

Theorem 1 (Uplink coverage for i.i.d. R_z): The uplink coverage probability $p_c(T, \lambda, \alpha, \epsilon)$ is given by:

$$2\pi\lambda \int_{r>0} r e^{-\pi\lambda r^2 - T r^{\alpha(\epsilon-1)}\sigma^2} \mathscr{L}_{I_z}\left(T r^{\alpha(1-\epsilon)}\right) \mathrm{d}r, \tag{4}$$

where the Laplace transform $\mathscr{L}_{I_z}(s)$ of the interference is given by

$$\exp\left(-2\pi\lambda \int_r^\infty \left(1 - \mathbb{E}_{R_z}\left[\frac{1}{1 + s R_z^{\alpha\epsilon} x^{-\alpha}}\right]\right) x \mathrm{d}x\right). \tag{5}$$

Proof: The coverage probability $p_c(T, \lambda, \alpha, \epsilon)$ can be expressed as a function of SINR as

$$\int_{r>0} \mathbb{P}\left(\text{SINR} > T\right) f_R(r) \mathrm{d}r \tag{6}$$

$$= \int_{r>0} \mathbb{P}\left(\frac{g\left(r^{\alpha(\epsilon-1)}\right)}{\sigma^2 + I_{\mathcal{Z}}} > T\right) 2\pi\lambda r e^{-\pi\lambda r^2} \mathrm{d}r \tag{7}$$

$$= \int_{r>0} \mathbb{P}\left(g > \frac{T(\sigma^2 + I_{\mathcal{Z}})}{r^{\alpha(\epsilon-1)}}\right) 2\pi\lambda r e^{-\pi\lambda r^2} \mathrm{d}r \tag{8}$$

$$\stackrel{(a)}{=} \int_{r>0} 2\pi\lambda r e^{-\pi\lambda r^2 - T r^{\alpha(1-\epsilon)}\sigma^2} \mathscr{L}_{I_z}\left(T r^{\alpha(1-\epsilon)}\right) \mathrm{d}r, \tag{9}$$

where (a) follows from the fact that $g \sim \exp(1)$ and $\mathscr{L}_{I_z}(s) = \mathbb{E}_{I_z}[e^{-sI_z}]$ is the Laplace transform of interference. To complete the proof, we now derive an expression for $\mathscr{L}_{I_z}(s)$ below:

$$\mathbb{E}_{I_z}\left[\exp\left(-\sum_{z\in\mathcal{Z}} s R_z^{\alpha\epsilon} g_z D_z^{-\alpha}\right)\right] \tag{10}$$

$$= \mathbb{E}_{R_z, g_z, D_z}\left[\prod_{z\in\mathcal{Z}} \exp\left(-s R_z^{\alpha\epsilon} g_z D_z^{-\alpha}\right)\right] \tag{11}$$

$$\stackrel{(a)}{=} \mathbb{E}_{R_z, D_z}\left[\prod_{z\in\mathcal{Z}} \mathbb{E}_{g_z}\left[\exp\left(-s R_z^{\alpha\epsilon} g_z D_z^{-\alpha}\right)\right]\right] \tag{12}$$

$$\stackrel{(b)}{=} \mathbb{E}_{D_z}\left[\prod_{z\in\mathcal{Z}} \mathbb{E}_{R_z}\left[\frac{1}{1 + s R_z^{\alpha\epsilon} D_z^{-\alpha}}\right]\right] \tag{13}$$

$$\stackrel{(c)}{=} \exp\left(-2\pi\lambda \int_r^\infty \left(1 - \mathbb{E}_{R_z}\left[\frac{1}{1 + s R_z^{\alpha\epsilon} x^{-\alpha}}\right]\right) x \mathrm{d}x\right), \tag{14}$$

where (a) follows from the independence of g_z, (b) follows from the independence of R_z and from the fact that

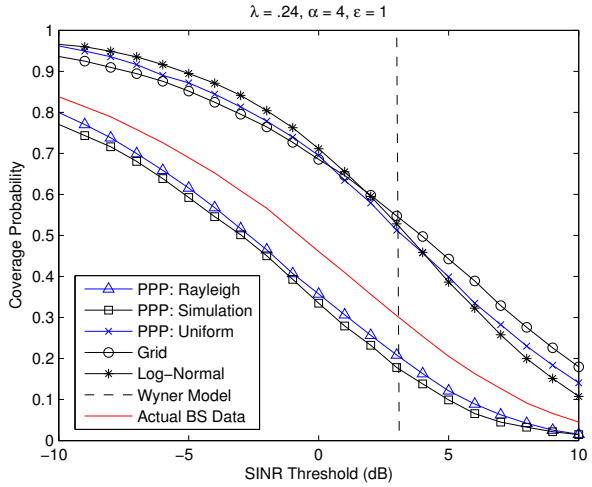

Fig. 3. A comparison of the uplink coverage probability for the proposed PPP-Rayleigh and PPP-Uniform models with numerical results for the grid and the PPP model (without independence assumption). Also included is the result using a set of actual BS locations and results using a log-normal approximation for the interference and the Wyner model with constant interference factor γ (assuming no-noise, $\alpha = 4,\ \epsilon = 1$).

$g_z \sim \exp(1)$ and (c) follows from the Probability Generating Functional (PGFL) of a PPP [10]. ■

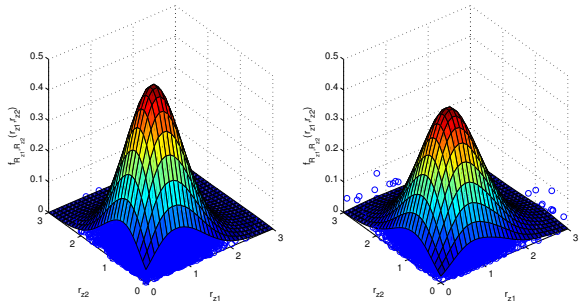

Fig. 4. 3-D view of the joint densities of R_{z_1} and R_{z_2} for the actual PPP model (left) and under the independence assumption (right). R_{z_1} and R_{z_2} are the distances of the mobiles to their respective BSs in two neighboring Voronoi cells.

A. Distribution of R_z and Comments on Independence Assumption

Recalling the fact that each BS is uniformly located in the Voronoi-cell of its corresponding mobile, the distribution of R_z can be approximated by the distance of a randomly chosen point in $\mathbb{R}^2$ to its closest BS as was done in the case of R. The pdf of R_z is then the same as R and is given by (3). The approximate CCDF of R_z is $\mathbb{P}[R_z > r_z] \approx e^{-\lambda\pi r_z^2}$, which is shown to be a tight fit for the numerical estimate for the PPP model in Fig. 2. Although it shows that our approximations for the distributions of R and R_z are tight, it does not provide any insight into the extent of dependence between random variables $\{R_z\}_{z\in\mathcal{Z}}$ which is defined by their joint distribution. Since it is hard to gain insights from the complete joint distribution of $\{R_z\}_{z\in\mathcal{Z}}$, we study a simplified case of the joint distribution of two random variables R_{z_1} and R_{z_2}, which are the distances of the mobiles to their respective BSs in two neighboring Voronoi cells. Since the dependence is expected to be strongest for the neighboring cells, this can be thought of as a worst case study. We numerically compute the joint PDF $f_{R_{z_1},R_{z_2}}(r_{z_1}, r_{z_2})$ for the actual PPP model and compare it with the joint PDF derived under the independence assumption in Fig. 4. It should be noted that the joint PDF under the independence condition follows directly from (3) and is given by $f_{R_{z_1},R_{z_2}}(r_{z_1}, r_{z_2}) = f_{R_{z_1}}(r_{z_1}) f_{R_{z_2}}(r_{z_2})$. From Fig. 4, we note that the two joint densities are surprisingly similar, with the PDF slightly more dispersed in the case of the independence assumption, which is the expected direct result of independence. The correlation coefficient $\rho_{R_{z_1},R_{z_2}}$ is numerically computed to be .07 for this simulation setup.

After validating the independence assumption, we now use the density of R_z derived above, to approximate the Laplace transform of interference for the PPP case, which is given by:

$$\mathscr{L}_{I_z}(s) \approx \exp\left(-2\pi\lambda \int_r^\infty (1-\mathcal{A})\, x\mathrm{d}x\right), \qquad (15)$$

where $\mathcal{A} = \int_0^\infty \frac{1}{1+su^{\frac{\alpha\epsilon}{2}} x^{-\alpha}} \pi\lambda e^{-\lambda\pi u}\mathrm{d}u$.

We note that the resulting coverage approximation involves two simple integrals that can be evaluated numerically fairly easily. We now plot this uplink coverage probability expression and compare it with the numerically computed coverage probability for a simulated PPP under true power control (without independence assumption) in Fig. 3. We note that the analytical result derived under the independence assumption closely approximates the true power control result for a PPP as well as the results based on simulations utilizing a set of actual BS locations compared to a regular grid.

The results in Fig. 3 are also further compared with two other analytical models. The first is the Wyner model which gives a single value for the interference and SIR $\equiv \frac{1}{2\gamma}$ where γ is a function of the pathloss exponent α [3] and as a result cannot model the typical performance in the same manner as the proposed model. The second approximates inter-cell interference as a log-normal random variable with parameters determined through a numerical fit of the grid model. The log-normal approximation provides a complete CCDF of the SINR, however it does not capture the shape of the SINR distribution. Additionally, since these approaches combine the interference into a single term that must be empirically estimated they cannot be easily parameterized as a function of key network features such as pathloss exponent, BS/user density, or fractional power control.

B. Comments on Regular (Grid) Model

Grid models are used to model more "regular" BS locations. The most popular model used in prior work places the BSs on a hexagonal grid. While this model has been extremely helpful in the numerical studies of macro-cellular networks, it does not provide analytical tractability. In this subsection, we show that the random spatial model for the mobile user locations along with an appropriately chosen distribution of R_z enables us to derive analytical expression for the coverage probability that

closely approximates the numerically computed results for the grid model.

Approximating hexagons as circles with the same area λ^{-1}, we assume that each BS is located uniformly in a circle of radius $\frac{1}{\sqrt{\pi\lambda}}$ around its corresponding mobile. The radius value is evaluated from the density of the mobile users assuming there is one BS per mobile user. It is important to note that the only difference between this and the original PPP model is the distribution of R_z, which is assumed to be uniform in $\left[0, \frac{1}{\sqrt{\pi\lambda}}\right]$ to emulate more regular networks. The density of R_z can be easily evaluated as:

$$f_{R_z}(r_z) = 2\pi\lambda r_z, r_z \in \left[0, \frac{1}{\sqrt{\pi\lambda}}\right]. \quad (16)$$

As shown in Fig. 2, this closely approximates the distribution of R_z in a grid model. Using this density of R_z, we can now approximate the Laplace transform $\mathscr{L}_{I_z}(s)$ of interference as:

$$\exp\left(-2\pi\lambda \int_r^\infty \left(1 - \int_0^\infty \frac{1}{1+su^{\alpha\epsilon}x^{-\alpha}} 2\pi\lambda u \mathrm{d}u\right) x \mathrm{d}x\right). \quad (17)$$

In the case of $\alpha = 4$ and $\epsilon = 1$ the expression for the Laplace transform $\mathscr{L}_{I_z}(s)$ can be found in closed-form as

$$e^{\left(-\frac{\pi\lambda}{2\sqrt{s}}\left(\pi\lambda \arctan\left(\frac{\sqrt{s}}{\pi\lambda r^2}\right) r^4 - \frac{s}{\pi\lambda}\arctan\left(\frac{\pi\lambda r^2}{\sqrt{s}}\right) - \frac{r^2}{\sqrt{s}} + \frac{s}{2\lambda}\right)\right)}. \quad (18)$$

We compare the coverage probability derived using this Laplace transform with the numerically computed coverage probability using true power control in a grid model in Fig. 3. Interestingly, we note that the analytical approximation closely resembles the true power control result for a hexagonal grid model. As was the case with the PPP model, a crucial step is to appropriately choose the distribution of R_z. Thus, while utilizing the same underlying random spatial model for the mobile user locations, we are able to "tune" the results to fit a range of highly non-uniform to very regular network topologies.

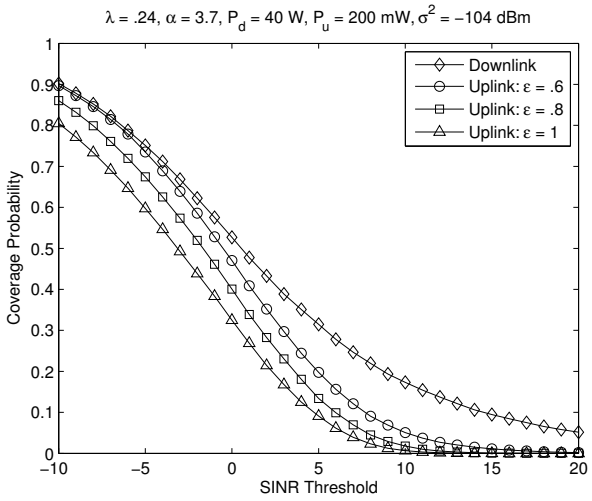

Fig. 5. A comparison of the coverage probability for the downlink with 40W transmit power and the uplink utilizing fractional power control with $\epsilon = .6, .8$ and 1, and a max transmit power of 200 mW.

IV. System Design Applications

Utilizing the framework developed in the previous section, we analyze performance metrics of coverage and transmit power utilization in the context of realistic parameters for modern networks and gain insight into system design.

A. Downlink vs. Uplink Coverage

An immediate application is to consider the difference in coverage between the downlink and the uplink for the same network topology.

Fig. 5 gives the coverage probability for the uplink and downlink based upon standard assumptions for an LTE-based network with $\lambda = .24$, $\alpha = 3.8$, $\sigma^2 = -104$ dBm [11]. The downlink expressions are given by [7] for a network whose BSs are distributed according to a PPP and transmit with constant power of 40 W. In the uplink a 23 dBm max transmit power is assumed with ϵ values of .6, .8, and 1. We note the disparity between the SINR distributions, especially for large SINR values. This has fundamental consequences on the system design of these cellular networks, different from those of wireless LANs for example which have much smaller coverage regions and typically do not have as significant hardware distinctions between the network devices.

One reason for the uplink's lower coverage is due to the mismatch in transmit power compared to the downlink. Additionally at the high SINR values, the use of larger ϵ values also impacts the coverage probability since the users closest to their serving base stations greatly reduce their transmit power relative to the users at the edge of the cell. The impact of ϵ is investigated in further detail in the following section.

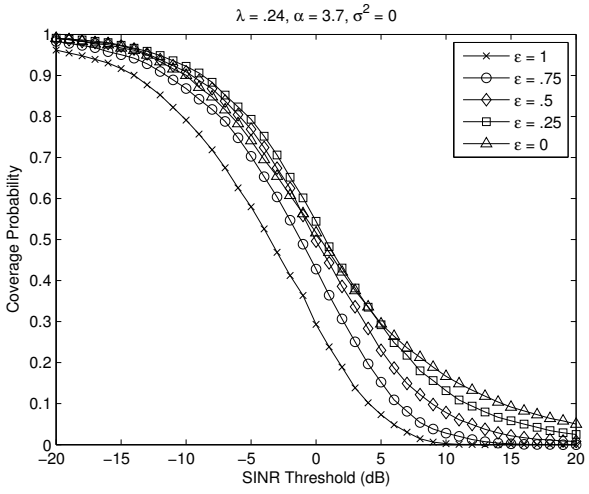

Fig. 6. A plot of the uplink coverage probability using the PPP-Rayleigh model for a range of ϵ values.

B. Fractional Power Control

As mentioned previously, the primary motivations for fractional power control in the cellular uplink are to provide beneficial coverage improvements for the lowest-percentile users, who are typically at the cell-edge, and to manage

average transmit powers of battery-powered mobile devices. Fig. 6 gives the coverage probability distributions as a function of the fractional power control factor ϵ for a network topology given by $\lambda = .24$, $\alpha = 3.8$, $\sigma^2 = -104$ dBm. The baseline case of fixed transmit power ($\epsilon = 0$) does not provide the lowest overall coverage probabilities, but does provide the greatest probability for the highest SINR thresholds. Both $\epsilon = .25$ and $\epsilon = .5$ provide greater coverage gains for the lowest percentile users than fixed transmit power before crossing below the $\epsilon = 0$ curve at 5 and 0 dB respectively. As ϵ increases, the coverage probability curves shift lower with $\epsilon = .75$ providing much lower coverage probability than fixed transmit power, especially for SINR thresholds > 5 dB. Full-inversion, $\epsilon = 1$ power control shows an even more significant reduction in coverage. For users with low SINR a moderate value of $\epsilon = .25$ provides the greatest gains while for users with high SINR, the SINR is maximized by transmitting with the maximum power and $\epsilon = 0$. Additionally, this dual-regime behavior for fractional power control in uplink cellular networks differs from the behavior of power control in other classes of wireless networks, notably ad-hoc wireless networks, which were shown to have an optimal value of $\epsilon = .5$ [12], [13].

This observed effect of fractional power control can be understood by focusing on the gains perceived by users close to their desired BS relative to those at the edge and their interdependency. Cell-interior users typically experience good RF conditions and are not as susceptible to interference, but are more limited by the reduction in their transmit power under power control. Cell-edge users, however, are more fundamentally interference limited, and an increase in their transmit power with high ϵ benefits their SINR. As a result, there is a trade off in the reduction of interference from neighboring cell-center users and increased interference by mobiles at the cell edge.

C. Transmit Power Utilization

Fig. 7 gives the overall transmit power utilization of mobiles in the network as a function of ϵ with a maximum transmit power of 23 dBm and an average transmit power of $\mu^{-1} = 10$ dBm. Clearly the transmit powers of the mobile users are greatly reduced with the introduction of power control. For high values of ϵ we note that 10-15% of the users have transmit power less than 0 dBm, which is a 23 dB reduction in power compared to the maximum transmit power. For this reason, proposed system guidelines for the uplink may wish to choose ϵ to balance the metrics of coverage and battery utilization.

V. Conclusion

In this paper, we have presented a tractable new model for cellular uplink analysis and derived a simple expression for coverage probability using tools from point process theory and stochastic geometry. Assuming mobiles form a spatial PPP, we model the correlation in mobile and BS point processes by assuming that each BS is located uniformly in the Voronoi cell of its corresponding mobile. The results further provide insight into differing uplink performance expectations compared to the downlink and the tradeoff between using fractional power control to reduce mobiles' overall power utilization and improving coverage for cell-edge users. A major arena for future work is to understand how these dynamics are enhanced or differ for heterogeneous network topologies.

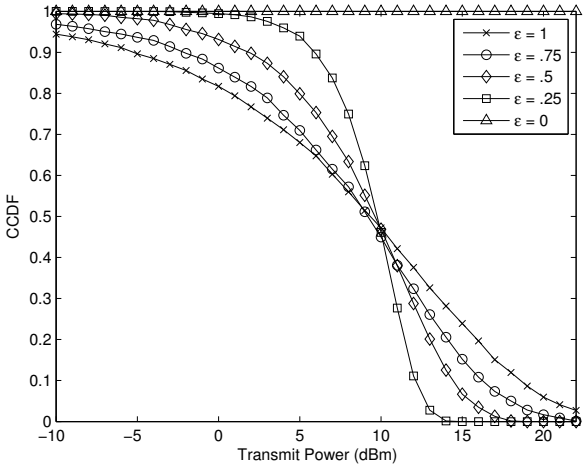

Fig. 7. The CCDF of the average transmit power per mobile as a function of ϵ with $\lambda = .24$, $P_{max} = 23$dBm, $\mu^{-1} = 10$dBm, and $\alpha = 3.7$ pathloss factor.

References

[1] Ericsson, "R1-074850: Uplink power control for E-UTRA - range and representation of P0," *3GPP TSG RAN WG1 Meeting #51*, Novemeber 2007.

[2] A. Wyner, "Shannon-theoretic approach to a Gaussian cellular multiple-access channel," *IEEE Transactions on Information Theory*, vol. 40, no. 6, pp. 1713–1727, Nov. 1994.

[3] J. Xu, J. Zhang, and J. Andrews, "On the accuracy of the Wyner model in cellular networks," *IEEE Transactions on Wireless Communications*, vol. 10, no. 9, pp. 3098–3109, Sep. 2011.

[4] R. Mullner, C. Ball, K. Ivanov, J. Lienhart, and P. Hric, "Contrasting open-loop and closed-loop power control performance in UTRAN LTE uplink by UE trace analysis," in *Proc. IEEE International Conference on Communications*, June 2009, pp. 1–6.

[5] M. Coupechoux and J. Kelif, "How to set the fractional power control compensation factor in LTE?" in *Proc. IEEE Sarnoff Symposium*, May 2011, pp. 1–5.

[6] H. S. Dhillon, R. K. Ganti, F. Baccelli, and J. G. Andrews, "Modeling and analysis of K-tier downlink heterogeneous cellular networks," *IEEE Journal on Selected Areas in Comm.*, Apr. 2012.

[7] J. Andrews, F. Baccelli, and R. Ganti, "A tractable approach to coverage and rate in cellular networks," *IEEE Transactions on Communications*, vol. 59, no. 11, pp. 3122–3134, Nov. 2011.

[8] S. Govindasamy and D. H. Staelin, "Asymptotic spectral efficiency of the uplink in spatially distributed wireless networks with multi-antenna base stations," 2011, available Online: http://arxiv.org/abs/1102.1232.

[9] D. B. Taylor, H. S. Dhillon, T. D. Novlan, and J. G. Andrews, "Pairwise interaction processes for modeling cellular network topology," in *Proc. IEEE Global Telecomm. Conference*, Anaheim, CA, Dec. 2012.

[10] D. Stoyan, W. Kendall, and J. Mecke, *Stochastic Geometry and Its Applications, 2nd Edition*. John Wiley and Sons, 1996.

[11] A. Ghosh, J. Zhang, J. G. Andrews, and R. Muhamed, *Fundamentals of LTE*. Prentice Hall, 2010.

[12] N. Jindal, S. Weber, and J. Andrews, "Fractional power control for decentralized wireless networks," *IEEE Transactions on Wireless Communications*, vol. 7, no. 12, pp. 5482 –5492, Dec. 2008.

[13] X. Wu, S. Tavildar, S. Shakkottai, T. Richardson, J. Li, R. Laroia, and A. Jovicic, "FlashLinQ: A synchronous distributed scheduler for peer-to-peer ad hoc networks," in *Allerton Conference on Communication, Control, and Computing*, Oct. 2010, pp. 514–521.